Atmospheric
Chemistry
and Physics

Open Access

On clocks and clouds

M. K. Witte[1], P. Y. Chuang[1], and G. Feingold[2]

[1]Earth and Planetary Sciences, University of California Santa Cruz, Santa Cruz, CA, USA
[2]Earth System Research Laboratory, Chemical Sciences Division, NOAA, Boulder, CO, USA

Correspondence to: M. K. Witte (mkwitte@ucsc.edu)

Abstract. Cumulus clouds exhibit a life cycle that consists of (a) the growth phase (increasing size, most notably in the vertical direction); (b) the mature phase (growth ceases; any precipitation that develops is strongest during this period); and (c) the dissipation phase (cloud dissipates because of precipitation and/or entrainment; no more dynamical support). Although radar can track clouds over time and give some sense of the age of a cloud, most aircraft in situ measurements lack temporal context. We use large eddy simulations of trade wind cumulus cloud fields from cases during the Barbados Oceanographic and Meteorological Experiment (BOMEX) and Rain In Cumulus over the Ocean (RICO) campaigns to demonstrate a potential cumulus cloud "clock." We find that the volume-averaged total water mixing ratio r_t is a useful cloud clock for the 12 clouds studied. A cloud's initial r_t is set by the subcloud mixed-layer mean r_t and decreases monotonically from the initial value due primarily to entrainment. The clock is insensitive to aerosol loading, environmental sounding and extrinsic cloud properties such as lifetime and volume. In some cases (more commonly for larger clouds), multiple pulses of buoyancy occur, which complicate the cumulus clock by replenishing r_t. The clock is most effectively used to classify clouds by life phase.

1 Introduction

Looking at the sky reveals immense variability in the properties and evolution of clouds, even those adjacent to one another. Variance among clouds is due not only to spatial variability in quantities such as temperature and humidity, but also to temporal variability – i.e., differences in cloud age. Fortunately, the overall evolutionary arc of clouds is roughly predictable. Shallow, warm cumuli begin as a pulse of pos-

itively buoyant air rising up through the boundary layer. As a cloud ages, the liquid water depletion processes (namely entrainment and precipitation) govern cloud dissipation. Past analyses of in situ observations have implicitly assumed that temporal variance is minimized by random sampling of many clouds of unknown age to paint a picture of an "average-aged" cloud. Yet inherent to cumulus evolution are distinctive stages defined by the different physical processes active during each. Knowing the age of a cloud then gives insight into which processes are expected to be most important at the time of observation. Furthermore, using in situ observations of cumulus to explore cloud–aerosol interactions or test theory is more meaningful if cloud age is known because it allows for testing representations of cloud mechanics at the process level.

In his essay "Of Clouds and Clocks", the philosopher Karl Popper presents clouds as a probabilistic, nonlinear system:

> My clouds are intended to represent physical systems which...are highly irregular, disorderly, and more or less unpredictable...On the other extreme...we may [consider] a very reliable pendulum clock, a precision clock, intended to represent physical systems which are regular, orderly, and highly predictable in their behaviour. (Popper, 1972)

While it is effectively impossible to predict a priori where an individual cumulus cloud will form or exactly how long it will last, all cumuli follow the same general progression as described above. Given this common framework for cloud evolution, the question then is whether there exists an orderly, predictable clock that is applicable to an unruly cloud population.

Observing the evolution of individual clouds in a field of cumuli is challenging. Because cumuli have an average

lifetime of less than an hour (Jiang et al., 2006; Dawe and Austin, 2011), estimating their age requires repeated observations every ~ 5 min. Ground-based remote sensors such as radar are capable of sampling at this frequency, but sacrifice sample volume in order to repeat quickly. Even with a 5 min repeat cycle, it may not be easy to accurately track clouds from one scan to the next. Reducing sample volume also increases the risk that clouds will depart the volume before the end of their lifetimes. Furthermore, scanning radar must contend with decreasing spatial resolution at increased distance from the sensor (Fielding et al., 2013). Lastly, cloud radar can not always accurately deduce critical cloud properties such as cloud liquid water content because measurements are strongly sensitive to the concentration of the largest drops, which is not necessarily correlated with other properties of interest. Nonetheless, cloud radar is likely the most effective observational tool for studying the life cycle of cumulus clouds.

Satellites have even stricter limitations for cloud life cycle studies. Geostationary satellite data is currently available at 15 min intervals at best, with a horizontal resolution of 1 km in the visible and 4 km in the IR spectrum for GOES. Such long repeat cycles and coarse spatial resolution make such observations unsuitable for examining small cumuli, but are appropriate for studying larger, longer-lasting clouds such as stratocumuli or deep cumuli. Satellites also have a limited arsenal of measurements: primarily droplet effective radius, cloud fraction, and cloud optical depth. Liquid water path (LWP) can be derived from the cloud optical depth and drop effective radius with the assumption of a liquid water content (LWC) profile.

Aircraft are able to make repeated measurements (1–2 min repeat cycle) of the same cloud, but given limits on flight time, repeated observation of just a few targets necessarily limits the ability to compile statistics of a cloud field. Multiple observations also rely on an a priori assumption of cloud age, that is, the cloud of interest must be young. If the cloud is first observed while dissipating, there may be nothing left for further observation. One key advantage of aircraft is the ability to measure a wide range of relevant cloud properties (temperature, LWC, drop size distribution, turbulence, etc.), but poor understanding of the temporal and spatial context of these measurements is a key limitation.

Our goal for this study is to assess whether there exists a method to infer the age of a cloud based on a single observation of that cloud. We define a good cloud "clock" as an observable quantity that assigns age based on a measurement at a single moment in time, regardless of the cloud's history. The most easily observed quantity, time elapsed since cloud nascence, is problematic. Time elapsed is an initial time subtracted from the present time, violating the requirement that age be determined from one measurement. Individual clouds vary greatly in lifetime, even those in close proximity to each other, due primarily to variations in the forcings and environment that each experiences. A 15 min old cloud could be

growing or dissipating. Thus, elapsed time alone provides ambiguous information about what is occurring at the process level. Instead, age is more readily framed in terms of cumulus life cycle phases: growth, maturity and dissipation. During the growth phase, the cloud increases in size, mostly in the vertical direction. As the cloud matures, the rate of growth slows and reverses; any precipitation that develops is strongest during this period. Finally, the cloud dissipates due to a combination of entrainment and precipitation reducing liquid water, while the lack of dynamical support shuts down the production of new liquid water. In order to accommodate clouds of different lifetimes, we use a non-dimensional time t/τ, where τ is cloud lifetime. All clouds are born at $t/\tau = 0$ and all clouds have fully dissipated by $t/\tau = 1$. If it were possible to follow a cloud in real time, such that birth and dissipation times were known, non-dimensional time would be an excellent candidate for the ideal cloud clock. Even this measure, though, is not perfect. Cloud life phases do not take equal amounts of non-dimensional time – the dissipation phase can happen gradually or catastrophically; rejuvenating pulses of buoyant air can occur in existing clouds, essentially reverting lucky clouds to the youthful growth phase (Heus et al., 2009).

Exploring whether a useful cloud clock exists is most easily achieved through the use of large eddy simulation (LES) of shallow cumulus fields to follow a diverse population of clouds over the course of their lifetime, from birth to dissipation. This allows for the evaluation of a wide range of potential clock candidate variables over the lifetime of numerous clouds, with a focus on what can be measured in situ by aircraft. Some remotely sensed quantities such as liquid water path can also be deduced from model output.

The description of cloud life phases above is most applicable to clouds that experience a single buoyancy pulse. However, some clouds experience multiple buoyancy pulses. Subsequent pulses cause ambiguity because growth in the lower part of the cloud can occur simultaneously with dissipation in the upper part of the same cloud. Thus no single life phase description is applicable.

Despite these challenges, it still appears worthwhile to evaluate the possibility of estimating cloud age from a "snapshot" observation. One important application is to approximately classify aircraft-observed clouds by life phase. We emphasize that to be useful, a clock need not be perfect; misclassification of some clouds is acceptable if most clouds are appropriately characterized.

2 Methodology

The study uses previously reported three-dimensional LES of trade wind cumuli based on cases from the Barbados Oceanographic and Meteorological Experiment (BOMEX, Xue and Feingold, 2006) and the Rain in Cumulus over the Ocean experiment (RICO, Jiang et al., 2009). The BOMEX

Table 1. Model details.

	BOMEX clean	BOMEX polluted	RICO
Model	UCLA-LES		Adapted RAMS
Grid $\Delta x, \Delta y, \Delta z$, m	100, 100, 40		50, 50, 20
Domain x, y, z, m	6400, 6400, 3000		6400, 6400, 4000
Cell size, m^3	4×10^5		5×10^4
Horizontal buffer, m	200		100
Δt, s	1.5		1.5
Simulation time, h	6		6
N_a, cm^{-3}	25	2000	100
Graph trace	Solid	Dash	Dash-dot
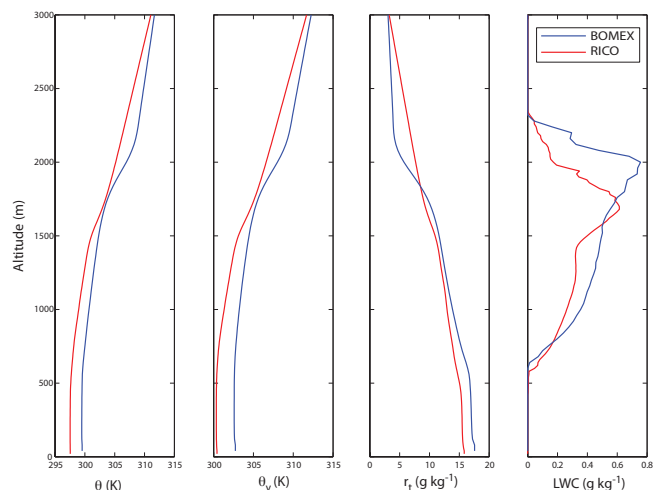
Figure 1. Environmental soundings taken over the period of time from which clouds are selected. With the exception of LWC, the profiles are clear-air domain averages.

simulations are further subdivided into clean and polluted cases. The models and relevant model parameters are described in Table 1 and environmental soundings are given in Fig. 1. Both models use periodic boundary conditions and are initiated with instantaneous pseudo-random temperature perturbations near their lowest levels. The first 3 h of each simulation are discarded as spin-up. Individual clouds are manually tracked over the course of their lifetime. For an overview of small cumulus evolution in LES, see Dawe and Austin (2011). A cloudy cell is defined as having liquid water content greater than 5×10^{-2} g kg^{-1} and a clear air cell is defined by LWC less than 1×10^{-18} g kg^{-1}. Any value between the thresholds is excluded from analysis, which accounts for < 1 % of all cells. Cloud lifetime is defined as the elapsed time during which the cloud comprises at least five contiguous cloudy cells such that clouds may initially form as a small number of nonadjacent cells. We define "contiguous" as sharing an adjoining face. Clouds were chosen such that a clear-air buffer exists around them throughout their lifetime to maintain individual cloud identity. The

buffer zone ensures a given cloud will not merge with any other cloud. Clouds that split horizontally into fragments and clouds with a minimum mature phase vertical extent of less than 200 m are also excluded from the study.

Each cloudy and clear cell is characterized by the following values: total water mixing ratio r_t, liquid water mixing ratio or liquid water content LWC, potential temperature θ, virtual potential temperature θ_v, and the resolved-scale vertical wind variance $\overline{w'^2}$, which is used as a proxy for turbulent kinetic energy. At each time step, the cloudy cell values are summed to give cloud total r_t, LWC, and $\overline{w'^2}$ as a preliminary step to computing cloud averages. The buoyancy perturbation $\Delta\theta_v$ is found by taking the difference between a cloudy value of θ_v and the clear air mean $\overline{\theta}_{v,clr}$ at the same altitude level. The value $\Delta\theta_v = \theta_v - \overline{\theta}_{v,clr}$ then is the buoyancy of cloudy air relative to the clear air around it. Positive values of cloud-average $\Delta\theta_v$ indicate positive buoyancy, while negative values indicate the opposite, which on average are associated with rising and subsiding motion, respectively.

In addition, some extrinsic properties of the cloud are determined: cloud volume, surface area, maximum cross-sectional area, depth, liquid water center of mass and liquid water path. Volume is the sum of contiguous cloudy cells at all vertical levels. Surface area is calculated by counting the number of cloudy cell surfaces abutting non-cloudy cells. Depth is the maximum number of contiguous cloud-populated altitude levels. Center of mass is the sum over the entire cloud of altitude times liquid water mass at each altitude divided by the total liquid water mass of the cloud. Liquid water path is estimated as the cloud-integrated LWC divided by maximum cross-sectional area. To directly compare clouds of varying size and lifetime, we scale the cloud characteristics (r_t, LWC, etc.) by the extrinsic cloud properties listed above (cloud volume, surface area, etc.) and normalize time by cloud lifetime τ.

In addition to cloud-integrated averaging, we derive altitude-specific variable averages to simulate an aircraft pass when cloud depth is greater than 200 m. Altitude averages were taken using normalized cloud height (where $z^* = 0$ corresponds to the instantaneous cloud base, $z^* = 1$ to the
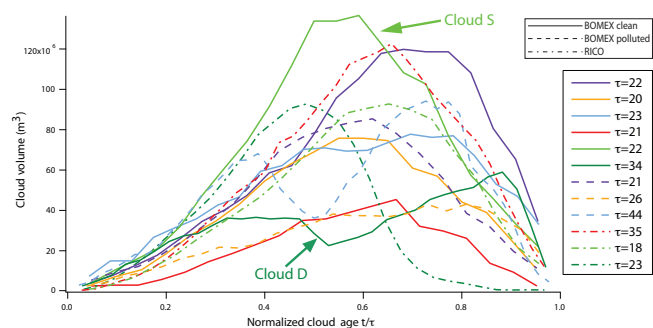
Figure 2. Cloud volume vs. normalized time. Lifetime τ is in minutes.

instantaneous cloud top) throughout the cloud. The normalized levels used are the nearest whole number altitude levels above cloud base ($z^* = 0.25$), at mid-cloud ($z^* = 0.5$) and below cloud top ($z^* = 0.75$). Since cloud base and top change over time, the single-level averages vary in absolute altitude over a cloud lifetime.

3 Results and discussion

3.1 The clouds

Overall, a total of twelve individual clouds are examined, four of which experienced a second buoyant pulse. Cloud lifetimes range from 18 to 44 min and maximum volume ranges from 4×10^7 to 1.4×10^8 m^3 (Fig. 2). Cloud base was between 640 m and 680 m for both the BOMEX and RICO simulations. Typical mature-stage cloud depth is approximately 1200 m. Six of the clouds are from the "clean" BOMEX simulation, three are from the "polluted" BOMEX simulation, and three are from the "clean" RICO simulation. Of the 12 clouds, only one (cloud S in Fig. 2) exhibits a lifetime-averaged rain rate greater than 1 mm day^{-1}.

As shown in Fig. 2, all clouds grew in volume from nascence until about $t/\tau \sim 0.3$, at which point single-pulse and double-pulse clouds diverged: all single-pulse clouds (e.g., cloud S in Fig. 2) continued to grow, reaching a maximum volume in the interval $0.5 < t/\tau < 0.8$ and subsequently dissipated. Double-pulse clouds (e.g., cloud D in Fig. 2) experienced some dissipation in the interval $0.4 < t/\tau < 0.6$, followed by a period of renewed growth and eventually dissipation.

There are divergent paths by which individual clouds dissipate. For example, clouds can dissipate from the base up, from the top down or from a combination of the two (model results not shown). At any altitude, dissipation along the cloud perimeter exhibits similar variability. This occurs because dissipation is not subject to the same constraints as nascence, whereby all clouds must grow upward from the lifting condensation level. Because there is no consistency in the evolution of clouds near the end of their lifetime, it is un-
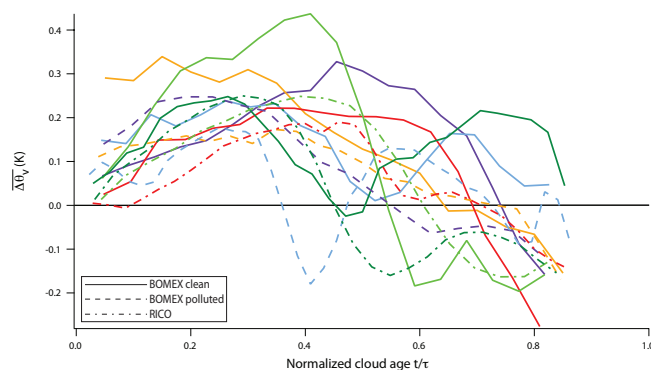
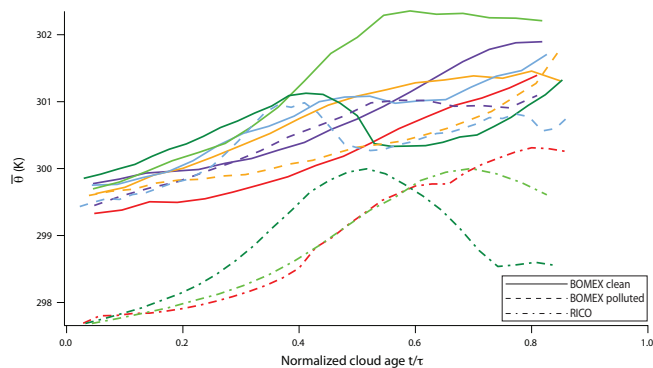**Figure 3.** Volume-averaged time series of $\Delta\theta_{\mathrm{v}}$.
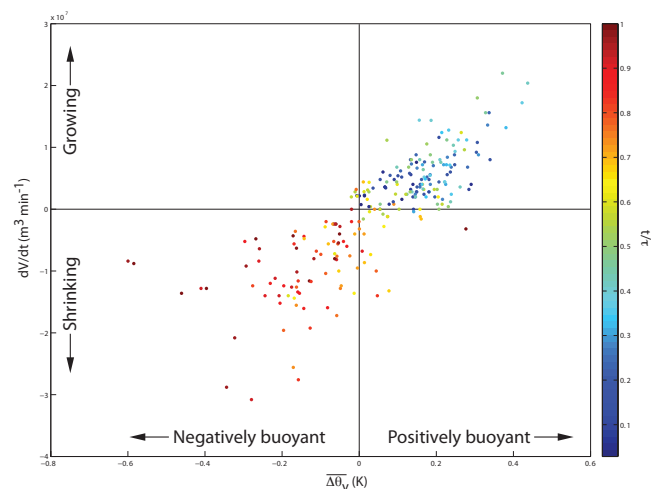
Figure 4. Scatter plot of volume-averaged $\Delta\theta_{\mathrm{v}}$ and $\frac{dV}{dt}$.

likely that there exists an accurate clock for this time period. For this reason we omit from our analyses $t/\tau > 0.9$, which corresponds to the final 3 to 5 min of cloud lifetime.

When a cloud initially forms, the air is warmer and has more water vapor than the surrounding clear air, giving it a strongly positive value of $\Delta\theta_{\mathrm{v}}$, as seen in Fig. 3. As the cloud grows older, $\Delta\theta_{\mathrm{v}}$ decreases and eventually becomes negative such that rising motion gives way to subsiding motion. As expected, the time series of $\Delta\theta_{\mathrm{v}}$ in Fig. 3 show growth (i.e., $\frac{dV}{dt} > 0$) when the cloud is positively buoyant (i.e., $\Delta\theta_{\mathrm{v}} > 0$ K) and dissipation when the cloud is negatively buoyant. Figure 4 illustrates the relationship. Analyzing only points with $|\Delta\theta_{\mathrm{v}}| \geq 0.05$ K, 93 % of the analyzed points in Fig. 4 lie within the upper-right and lower-left quadrants, indicating a robust correlation between growth and buoyancy. Comparing the volume and $\Delta\theta_{\mathrm{v}}$ time series of cloud D (Figs. 2 and 3) illustrates that this correlation holds for multiple-pulse clouds.

Table 2. Intrinsic and extrinsic variables examined.

Intrinsic		Extrinsic (relative to cloud)
Total water mixing ratio	r_t	Depth
Liquid water mixing ratio/content	LWC	Area
Potential temperature	θ	Maximum cross-sectional area
Virtual potential temperature	θ_v	Surface area
Moist static energy	MSE	Volume
Vertical velocity variance	$\overline{w'^2}$	Liquid water path
		Liquid water center of mass

Figure 5. Time series of volume-averaged potential temperature.
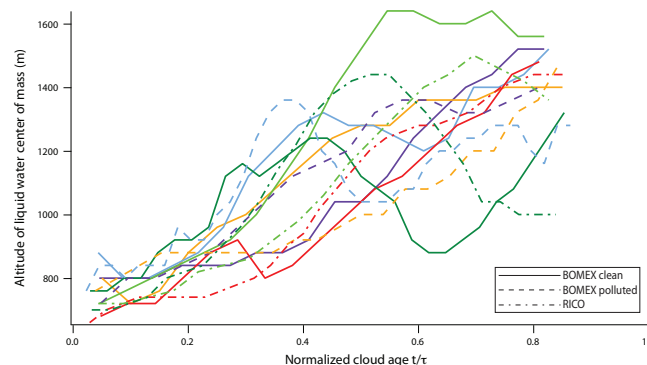
Figure 6. Time series of the altitude of liquid water cloud center of mass.

3.2 The ideal clock

The ideal cloud clock must account for variation in both cloud extrinsic properties (i.e., lifetime and size) and environmental conditions. The former is minimized by normalizing time and utilizing intrinsic rather than extrinsic cloud properties. Some techniques to account for variability in environmental conditions are explored in Sect. 3.4. Schematically, the ideal clock is a monotonic function of time, whereby a single measurement of a cloud (by aircraft) can be used to infer a narrow range of *normalized* age.

3.3 Failures

Table 2 lists all the potential clock variables and averaging quantities analyzed. All possible combinations were examined. Potential clock variables fail for a variety of reasons. For example, potential temperature shows a slight increasing trend over time (Fig. 5), but the dynamic range is small, with θ varying by about 1 % of the initial value over cloud lifetime. The poor dynamic range implies that a combination of sampling variability and measurement uncertainty translates to a highly uncertain age estimate. The buoyancy perturbation $\Delta\theta_v$ does not work as a clock because the individual cloud magnitude is dependent on cloud volume and time series are multi-valued, even for single-pulse clouds (Fig. 3). The altitude corresponding to the cloud liquid water center of mass (Fig. 6) functions reasonably as a clock because it

monotonically increases over time. In practice, though, measuring center of mass in situ is not plausible; it could be achieved by rapidly scanning cloud radar and an assumed Z–LWC relationship. The latter problem has been explored elsewhere (e.g., Koren et al., 2009). As shown in Fig. 7, cloud top height operates in a qualitatively similar manner to center of mass, is multivalued for all analyzed clouds, and for older clouds ($t/\tau > 0.3$) estimates cloud age with poor accuracy.

3.4 Total water as cumulus clock

Assuming adiabatic lifting, the value of the total water mixing ratio r_t at cloud base during cloud nascence is approximately equal to the mixed layer value $r_{t,ml}$. Normalizing time series of r_t by the domain-averaged mixed layer value $\overline{r_{t,ml}}$ yields the normalized total water $r_t^* \equiv r_t/\overline{r_{t,ml}}$, which allows for comparison between different atmospheric conditions. Initial values of r_t^* are approximate unity because clouds form from pulses of buoyant mixed-layer air. It is possible that initial values of cloud-averaged r_t^* may be greater than unity because of spatial variability in the r_t field.

For all clouds, the volume-averaged time series of r_t^* initially ($t/\tau < 0.4$) decreases monotonically (Fig. 9, upper left). We attribute this decrease to entrainment rather than precipitation. For shallow trade-wind convection (Stevens, 2005), environmental r_t generally decreases with altitude above the surface mixed layer. Hence mixtures of entrained
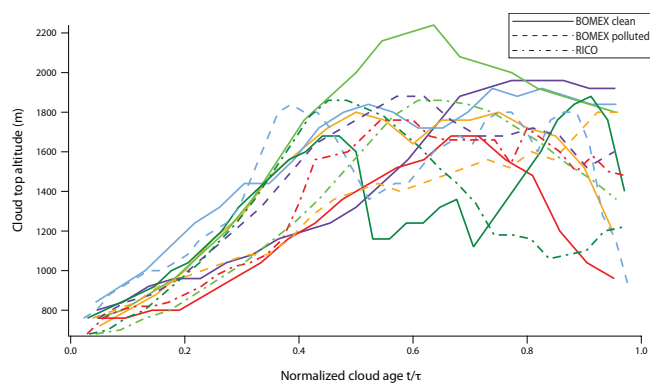
Figure 7. Time series of cloud top altitude.
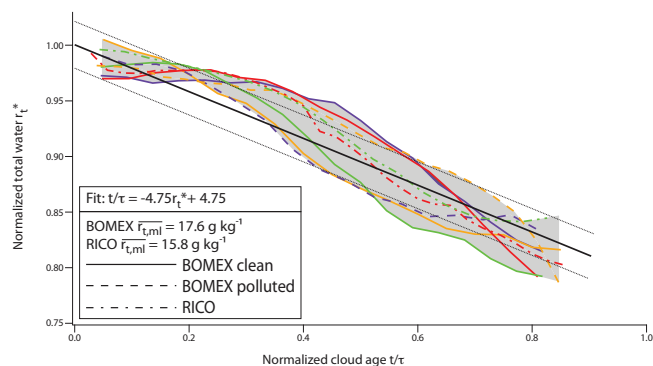
Figure 8. The time evolution of r_t^* is well fit by linear regression. The solid black line is the fit and the dashed black lines are approximately one standard deviation from the mean slope.

and mixed-layer air will have lower r_t than the pure mixed-layer air that initially comprises the cloud. If the decrease were instead due to precipitation, r_t^* would be approximately constant during the growth phase and only begin to decrease during the mature phase when the cloud is sufficiently deep enough for precipitation to develop. However, r_t^* begins to decrease immediately, indicating that entrainment likely dominates the r_t^* trend. We further address the impact of precipitation in Sect. 3.5.

3.4.1 Single-pulse clouds

For single-pulse clouds, r_t^* monotonically decreases throughout cloud lifetime, as shown in Fig. 8. The clouds dissipate once total water is less than saturation. In between, the slope of r_t^* is fairly linear [1] ($R^2 = 0.88$) among single-pulse clouds: the mean slope and standard deviation are $-0.23 \pm$

---

[1]The data are better fit by a parabola ($R^2 = 0.93$), but we chose to use the simplest possible fit because of the small sample size. One possible explanation for a parabolic curve is that when a cloud is young and shallow, the difference between environmental and cloud r_t is small, while as the cloud ages and deepens, the r_t contrast grows.

0.06, respectively, with R^2 for individual clouds ranging from 0.88 to 0.97. This indicates that entrainment causes drying at an approximately fixed rate with respect to normalized time, independent of maximum volume and lifetime. In some respects, this is not surprising. All clouds begin around $r_t^* \sim 1$, while the final r_t^* value should be the saturation water vapor mixing ratio. Over the lifetime of each cloud, the decrease in r_t^* is constrained between these two values. Thus the slope with respect to normalized time is not able to vary widely. Some variance of the slope is expected due to variation in final r_t^* values. This occurs because clouds dissipate at different altitudes, corresponding to different temperatures and hence different saturation mixing ratios.

Because r_t^* monotonically decreases in an approximately linear fashion, we propose that it can be used as a cumulus clock. As illustrated in Fig. 8, a cloud with mean $r_t^* = 0.9$ is predicted to have an approximate age of $t/\tau = 0.48 \pm 0.10$. This age uncertainty of $\Delta(t/\tau) \sim 0.1$ represents approximately one standard deviation and is consistent over a cloud lifetime. This uncertainty is sufficiently low for a reasonable estimation of the life phase of single-pulse clouds. The age model applies equally to the RICO and BOMEX meteorological soundings, the clean and polluted BOMEX clouds, and to clouds of differing lifetime and volume, suggesting that it may be generalizable to shallow cumulus in a variety of environments. Further study is necessary to better understand the range of environmental conditions to which the clock may be applied.

Up to this point, the r_t^*-based clock has used cloud-averaged r_t^* values. However, for aircraft observations, it is desirable to infer cloud age from a single aircraft pass. The monotonic decrease in r_t^* with time evident in the cloud-averaged time series (Fig. 8) is also seen in the time series of r_t^* at selected normalized cloud layer levels $z^* = 0.25$; 0.50; and 0.75 where $z^* = 0$ corresponds with instantaneous cloud base and $z^* = 1$ is instantaneous cloud top (Fig. 9). The variability of r_t^* among single-pulse clouds is also similar between cloud-averaged and single-level time series. The primary difference among the different levels is that the final value of r_t^* decreases with altitude because environmental r_t decreases with altitude. In addition, the colder temperatures near the cloud top can sustain saturation at lower r_t^* values than near the cloud base. As a result, there is a greater dynamic range in the time series of r_t^* at the cloud top than at the cloud base. The time series at $z^* = 0.50$ closely follow the cloud-averaged time series upon which the clock is based, suggesting that it is most accurate to infer cloud age from single-level cloud passes at mid-cloud.

3.4.2 Multiple-pulse clouds

In those periods where a cloud exhibits increases in r_t^* with time, the cloud is experiencing a second buoyancy pulse, bringing with it moisture-rich mixed layer air. Cloud average r_t^* cannot return to its initial value near unity because it is
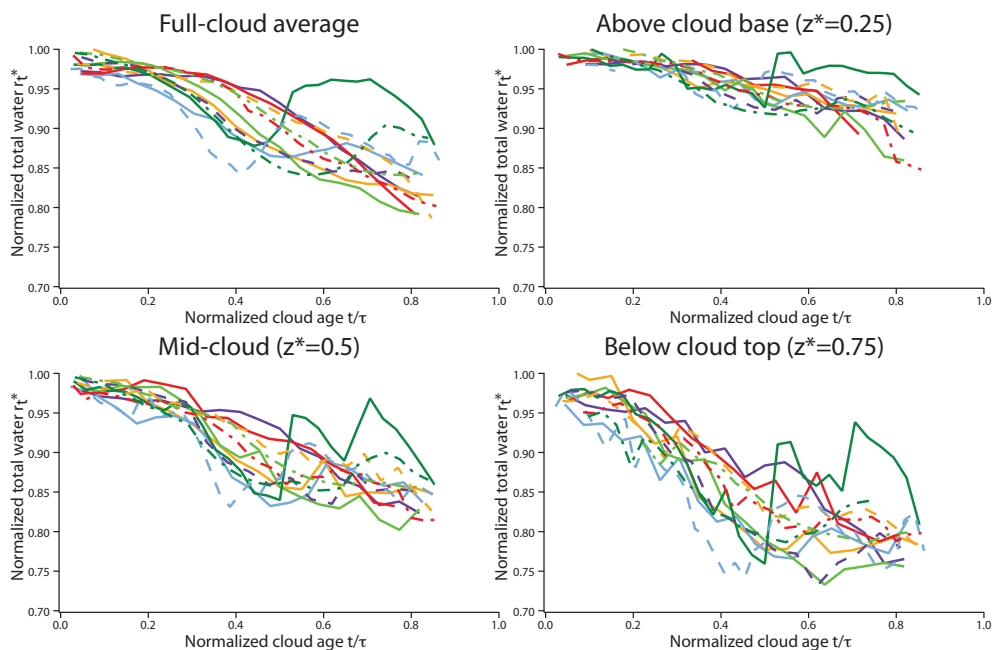
Figure 9. Individual altitude time series of r_t^* show the same general trend as the full-cloud average, but higher altitudes exhibit a larger dynamic range.
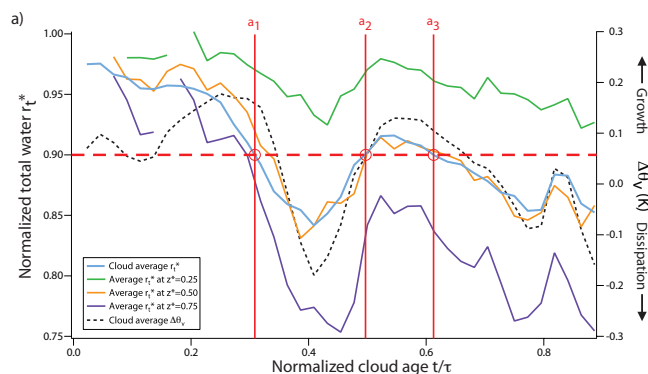

Figure 10. Time series of r_t^* averaged over the entire cloud and at individual levels. Cloud average $\Delta\theta_v$ is shown for comparison.

a cloud-integrated value with "memory" of past entrainment drying. After the influx of moisture, r_t^* again decreases via entrainment until cloud dissipation. Multiple pulses appear to extend cloud lifetime. The median lifetime of the single-pulse clouds analyzed is 22 min, with a range of 18 to 35 min. The two most obvious multiple-pulse clouds last for 34 and 44 min. While multiple-pulse clouds have a longer lifetime than single pulse clouds, they are still constrained to an initial value of $r_t^*(0) \sim 1$ and a dissipation value approaching the saturation vapor mixing ratio.

Interpretation of inferred age is more complicated for multiple-pulse clouds. Figure 10 illustrates r_t^* and $\Delta\theta_v$ for one multiple-pulse cloud with a "measurement" of $r_t^* \approx$

0.90. The single-pulse age model predicts an age of $t/\tau \approx 0.5 \pm 0.1$, while the cloud exhibits $r_t^* \approx 0.90$ three times ($a_1 \sim 0.3, a_2 \sim 0.5, a_3 \sim 0.6$, where a_i are the times at which hypothetical measurements were taken). Heus et al. (2009) (hereafter H09) interpret and analyze multiple pulses within a single cloud as independent events. Following the interpretation of H09, the inferred ages at times a_1 and a_3 can be viewed as *equivalent ages* for independent single pulses. This interpretation is supported by the comparison of the cloud-averaged r_t^* and $\Delta\theta_v$ in Fig. 10, which shows similar behavior at times a_1 and a_3. In both cases, $\Delta\theta_v$ is similar in value and decreases from a local maximum, suggesting *dynamical similarity*. Thus it is appropriate that the inferred clock age should be the same at times a_1 and a_3. Assuming the two pulses are independent, we can determine an independent single pulse age associated with each pulse. The times a_1 and a_3 can be expressed as single pulse ages b_1 and b_2, respectively. In Fig. 11, we approximate the respective single pulse time axes and roughly estimate the independent pulse ages $b_1 \approx 0.6 \pm 0.1$ and $b_2 \approx 0.4 \pm 0.1$. The estimates for b_1 and b_2 agree reasonably well with the inferred single-pulse age $t/\tau \approx 0.5 \pm 0.1$.

In the time period surrounding time a_2 ($0.4 \lesssim t/\tau \lesssim 0.5$, Fig. 10), r_t^* increases with time. The increase occurs gradually not only in the average, but also at individual levels of the cloud (Fig. 10), albeit for different durations (between 3 and 6 min). Although r_t^* begins to increase at different times for different levels, the second peak in r_t^* is reached at approximately the same time ($t/\tau \sim 0.5$) at each individual level, shown in Fig. 10. Detailed examination of cloud evolution

b)
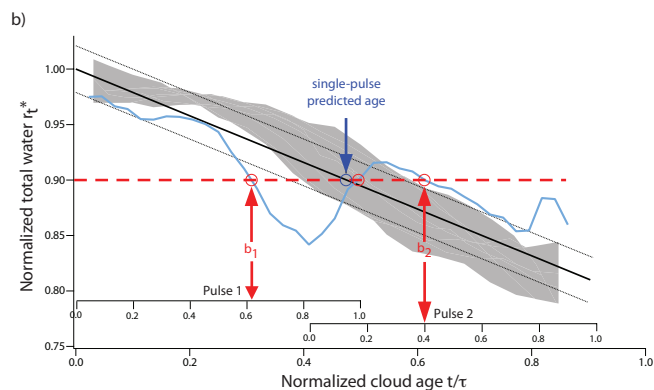
Figure 11. A cloud-averaged r_t^* time series for a double-pulse cloud. The solid black line is the single-pulse fit, the dashed black lines are the fit $t/\tau \pm 0.1$, and the gray area envelops the single-pulse cloud data. The Pulse 1 and Pulse 2 time axes show the independent pulse ages associated with times b_1 and b_2, respectively.
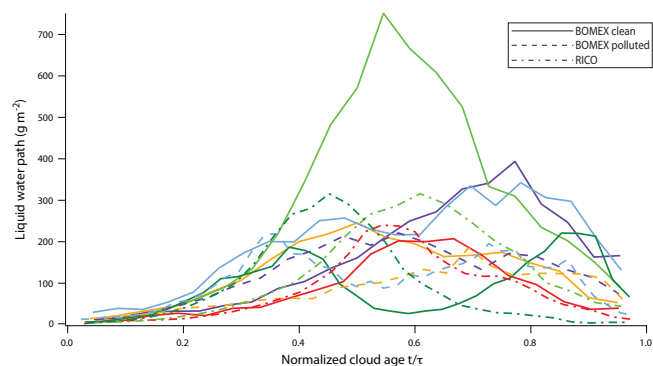
Figure 12. Time series of liquid water path. Liquid water path is the cloud-integrated LWC divided by maximum cross-sectional area.

shows that there are multiple reasons for the r_t^* increase. The second pulse begins near the cloud base and propagates upward, bringing high r_t^* air to the cloud. At the same time, dissipation occurs at the cloud top, which removes the lowest r_t^* values from the cloud because these values are found at the coldest temperatures/highest altitudes. No single age appropriately captures the dynamical complexity during the increase in r_t^* because, unlike the initial pulse that created the cloud, growth and dissipation occur concurrently at different regions in the cloud. The time period surrounding a_2 is neither a clear growth nor dissipation phase.

The r_t^* clock can be used to sort clouds by life phase, in conjunction with the knowledge that a cloud is growing when $\Delta\theta_v > 0\,\mathrm{K}$ and dissipating when $\Delta\theta_v < 0\,\mathrm{K}$ (Fig. 4). We propose that clouds can be designated as being in the growth phase when $r_t^* > 0.95$ and $\Delta\theta_v > 0\,\mathrm{K}$, and in the dissipation phase when $r_t^* < 0.85$ and $\Delta\theta_v < 0\,\mathrm{K}$. The variable space in between these boundaries is by default classified as the mature phase. Applying these criteria to all the clouds, 113 of 350 total sampled cloud time steps are classified as

"growth" phase and 73 of 350 are classified as "dissipation" phase. The remaining 177 time steps are classified as mature. Of the 113 growth phase time steps, 103 are associated with cloud age $t/\tau < 0.4$ and the remaining 10 time steps with the second pulse of a multiple-pulse cloud. Of the dissipation phase time steps, 60 of the 73 are associated with cloud age $t/\tau > 0.7$ and the remaining 13 with dissipation preceding the second pulse of two multiple-pulse clouds. The advantage of classifying clouds by life phase is that it resolves the issue of attributing a unique normalized age to multiple-pulse clouds, enabling the diagnosis of multiple growth and dissipation phases in a single lifetime. The most subsequent pulses will be classified as mature phase, though, because of the dynamical complexity inherent to multiple-pulse clouds discussed above.

In summary, the normalized age model inferred from time series of cloud average r_t^* predicts normalized age within $\Delta t/\tau \sim 0.1$ for single-pulse clouds and sorts all clouds into the growth and dissipation phases. The r_t^* clock is applicable to multiple-pulse clouds if the evolution of such clouds is viewed as a series of independent single pulses, in other words, if the cloud lifetime is subdivided into pulse lifetimes as in Fig. 11. From this perspective, each successive measurement of the same r_t^* value corresponds with a unique independent pulse age, regardless of the cloud's history. The transition period (or periods) between pulses during which r_t^* increases is dynamically complex and does not fit into the simple three-phase view of the cumulus life cycle, as clouds can display characteristics of all three phases during those time spans.

3.5 Caveats and limitations

We attribute the loss of total water over cloud lifetime mainly to entrainment. However, this loss can also be expressed as an equivalent lifetime-average rain rate on the order of $1\,\mathrm{cm\,h^{-1}}$. Rain rate was derived using the relationship $R \sim LWP^\alpha N_D^\beta$ with $\alpha = 2.5$ and $\beta = -1$ (Jiang et al., 2010). Of the 12 clouds analyzed, 9 exhibit a lifetime-average of $R \ll 1\,\mathrm{mm\,h^{-1}}$ and thus precipitation is negligible compared to entrainment. The most heavily precipitating cloud exhibits a lifetime-average of $R \sim 2\,\mathrm{mm\,h^{-1}}$, which is a factor of five smaller than the entrainment equivalent water loss. From these results, we infer that entrainment, and not precipitation, is the primary mechanism for liquid water depletion for the clouds sampled. Whether or not the r_t^* clock is applicable to deeper, more heavily precipitating clouds remains an open question.

We speculate that heavy precipitation would not substantially affect the utility of the r_t^* clock. As discussed above, the slope of the clock depends on the initial and final values of r_t^*. The initial value is constrained to be near unity, while the final value depends on the saturation vapor mixing ratio, which is a function of temperature. Cloud dissipation dominated by entrainment can lead to cooler temperatures relative

to dissipation dominated by precipitation. Entrainment mixes colder environmental air into the cloud and causes cloud drop evaporation. Precipitation reduces the potential for evaporative cooling by cloud droplet evaporation, leading to warmer cloud dissipation temperatures. We estimate that heavy precipitation would increase the final value of r_t^* by a few hundredths at most, less than the variability observed among the analyzed clouds (Fig. 8). Hence heavy precipitation would not dramatically alter the slope of r_t^* with respect to normalized time (but presumably would reduce cloud lifetime τ) and thus the r_t^* clock may also be applicable in such situations.

There are some caveats associated with the results of this study. First, the effective dynamical age inferred from the r_t^* clock does not accurately represent time-integrative processes like collision-coalescence, which are not reversible by subsequent buoyancy pulses. While such pulses act to "turn back" the r_t^* clock, the cloud drop size distribution does not experience a similar reversal, that is, the large drops formed by collision-coalescence are unlikely to shrink or disappear.

The 12 clouds examined are not a large set from which to draw generalized conclusions about all small cumuli. Since the clouds were selected by a human observer, it is possible that the selection process was biased. In particular, the clouds chosen for the study were more spatially isolated than the average cloud in the domain. While the selection was biased toward more isolated clouds, a BOMEX simulation by Dawe and Austin (2011) found that the majority of clouds form and decay in isolation (75 % and 89 % of all simulated clouds, respectively). To gain a more statistically robust sampling, the cloud tracking algorithm of Dawe and Austin (2011) could be employed. Furthermore, the differences between modeled and real small cumulus may impact these results. For example, there is disagreement in the representation of entrainment and detrainment mixing among different LES models (de Rooy et al., 2013). Because the r_t^* clock relies on moisture reduction, differences in how entrainment mixing and subsequent drying are represented may alter the operation of the clock.

4 Conclusions

The goal of this study is to find an observationally relevant, single-measurement cumulus clock. The purpose of the clock is to classify clouds by life phase, hence giving temporal context to observations of such clouds. We find that for LES-modeled shallow trade wind cumulus clouds, the normalized total water mixing ratio r_t^* (defined as the measured total water mixing ratio r_t normalized by the average mixed layer value $\overline{r_{t,ml}}$) can be used as a clock. It works because the cloud is initially moisture-rich ($r_t^* \sim 1$), but over time, entrainment of surrounding, drier environmental air causes r_t^* to decrease with time. The simulated clouds exhibit low lifetime-average rain rates ($R < 3\,\mathrm{mm\,d^{-1}}$). The operation

of the clock is insensitive to aerosol loading, environmental sounding and extrinsic cloud properties such as lifetime and volume. In the simplest case of a single-pulse cloud, interpretation of the clock provides a basis for classification of clouds by life phase. Clouds can be designated as being in the growth phase when $r_t^* \gtrsim 0.95$ and $\Delta\theta_v > 0\,\mathrm{K}$, and in the dissipation phase when $r_t^* \lesssim 0.85$ and $\Delta\theta_v < 0\,\mathrm{K}$. In between, clouds are by default classified as mature.

Interpretation of the age model is more complicated for multiple-pulse clouds. The effect of subsequent pulses generally acts to increase the buoyancy contrast $\Delta\theta_v$, altering the growth rate of the cloud and causing r_t^* to increase with time for some duration before entrainment again dominates the evolution. During periods when r_t^* is decreasing, we interpret the clock as an approximate "pulse-age" rather than "cloud-age" following Heus et al. (2009), who describe pulses as independent entities. The degree to which pulses can be considered independent, such that the influence on the cloud of older pulse(s) is minimal relative to the most recent pulse, is still an open question. During periods when r_t^* is increasing, the bottom and top portions of the cloud are dynamically distinct so no single "cloud-age" or life-phase description is sensible. Such cases confound the simple growth/mature/dissipation classification system.

We find the clock to be robust for the modeled clouds sampled, but we emphasize that the small, potentially biased population analyzed here does not provide sufficient evidence that the r_t^* clock can be applied universally to all small cumuli. Most importantly, the functionality of the clock in heavily precipitating conditions is unclear. Secondly, the r_t^* clock is not able to accurately record time-integrative processes such as collision-coalescence. Finally, splitting and merging clouds were intentionally not characterized. The applicability of the r_t^* clock may be limited in conditions conducive to significant splitting and merging among the cloud population. The utility of the clock and the seriousness of the caveats identified here could be tested by repeated aircraft sampling of a single cloud over its lifetime.

While the r_t^* small cumulus clock is not perfect, especially in the case of multiple-pulse clouds, it does appear to accurately classify the clouds sampled for this study in the growth and dissipation phases. In between, clouds classified as "mature" exhibit a wider range of behavior and thus dynamical (and other) similarity is not guaranteed. Even this basic classification, confounding Karl Popper's juxtaposition of clouds and clocks, could provide important and useful context for in situ cloud observations.

References

Dawe, J. T. and Austin, P. H.: Statistical analysis of an LES shallow cumulus cloud ensemble using a cloud tracking algorithm, Atmos. Chem. Phys., 12, 1101–1119, doi:10.5194/acp-12-1101-2012, 2012.

de Rooy, W., Bechtold, P., Fröhlich, K., Hohenegger, C., Jonker, H., Mironov, D., Siebesma, A., Teixeira, J., and Yano, J.-I.: Entrainment and detrainment in cumulus convection: an overview, Q. J. Roy. Meteor. Soc., 139, 1–19, 2013.

Fielding, M., Chiu, J., Hogan, R., and Feingold, G.: 3D cloud reconstructions: Evaluation of scanning radar scan strategy with a view to shortwave radiation closure, J. Geophys. Res., 118, 9153–9167, doi:10.1002/jgrd.50614, 2013.

Heus, T., Jonker, H., Van den Akker, H., Griffith, E., Koutek, M., and Post, F.: A statistical approach to the life cycle analysis of cumulus clouds selected in a virtual reality environment, J. Geophys. Res., 114, D06208, doi:10.1029/2008JD010917, 2009.

Jiang, H., Xue, H., Teller, A., Feingold, G., and Levin, Z.: Aerosol effects on the lifetime of shallow cumulus, Geophys. Res. Lett., 33, L14806, doi:10.1029/2006GL026024, 2006.

Jiang, H., Feingold, G., and Koren, I.: Effect of aerosol on trade cumulus cloud morphology, J. Geophys. Res., 114, D11209, doi:10.1029/2009JD011750, 2009.

Jiang, H., Feingold, G., and Sorooshian, A.: Effect of Aerosol on the Susceptibility and Efficiency of Precipitation in Warm Trade Cumulus Clouds, J. Atmos. Sci., 67, 3525–3540, 2010.

Koren, I., Altaratz, O., Feingold, G., Levin, Z., and Reisin, T.: Cloud's Center of Gravity – a compact approach to analyze convective cloud development, Atmos. Chem. Phys., 9, 155–161, doi:10.5194/acp-9-155-2009, 2009.

Popper, K.: Objective Knowledge: An Evolutionary Approach, Oxford University Press, USA, revised edn., 1972.

Stevens, B.: Atmospheric Moist Convection, Annu. Rev. Earth Planet. Sci., 33, 605–643, 2005.

Xue, H. and Feingold, G.: Large-Eddy Simulations of Trade Wind Cumuli: Investigation of Aerosol Indirect Effects, J. Atmos. Sci., 63, 1605–1622, 2006.